SAND2015-2676C

Radome Effects on Coherent Change Detection Radar Systems

Ann Marie Raynal,* Dale F. Dubbert, Bryan L. Burns, and William H. Hensley, Jr.
Sandia National Laboratories, PO Box 5800, Albuquerque, NM, USA 87185-0519

ABSTRACT

A radome, or radar dome, protects a radar system from exposure to the elements. Unfortunately, radomes can affect the radiation pattern of the enclosed antenna. The co-design of a platform's radome and radar is ideal to mitigate any deleterious effects of the radome. However, maintaining structural integrity and other platform flight requirements, particularly when integrating a new radar onto an existing platform, often limits radome electrical design choices. Radars that rely heavily on phase measurements such as monopulse, interferometric, or coherent change detection (CCD) systems require particular attention be paid to components, such as the radome, that might introduce loss and phase variations as a function of the antenna scan angle. Material properties, radome wall construction, overall dimensions, and shape characteristics of a radome can impact insertion loss and phase delay, antenna beamwidth and sidelobe level, polarization, and ultimately the impulse response of the radar, among other things, over the desired radar operating parameters. The precision-guided munitions literature has analyzed radome effects on monopulse systems for well over half a century. However, to the best of our knowledge, radome-induced errors on CCD performance have not been described. The impact of radome material and wall construction, shape, dimensions, and antenna characteristics on CCD is examined herein for select radar and radome examples using electromagnetic simulations.

Keywords: SAR, CCD, Synthetic Aperture Radar, Coherent Change Detection, Radome

1. INTRODUCTION

Coherent change detection (CCD) estimates subtle magnitude and phase differences between repeat-pass synthetic aperture radar (SAR) images of a scene. CCD is an interferometric technique whose goal is to minimize all decorrelation contributions from the radar and platform in order to have the maximum ability to highlight temporal decorrelation from the desired scene. Radar domes (or radomes) protect a radar system from weather and debris. Alas, no matter how well-designed electrically, radomes impact the radiation pattern of an antenna. Thus, ground imaging radars must consider antenna beamwidth and sidelobe level degradation, depolarization, reflections, insertion loss and phase delay effects of a radome.[1-2] The apparent antenna beamwidth can widen and sidelobe levels can increase through the radome, changing impulse response characteristics. Energy can be rotated into different polarizations than the transmitted one, resulting in an additional source of loss on receive. Radio-frequency power can be reflected from the radome wall into the antenna. A reduction in signal strength and phase differences can occur by insertion losses and phase delays through the radome wall. Radome losses not only reduce the main beam gain of the antenna through transmission loss but also increase noise. Signal-to-noise ratio degradation in turn impacts no-return area reflectivity levels, target detection, and coherence. Additionally, radomes are tied to an airborne platform's body angles, which are modified by navigational requirements as ambient factors, such as winds, change during flight. Therefore, the radome moves independently of the actual antenna pointing carried-out by the radar to perform ground imaging. Consequently, the antenna of CCD systems may look out different sectors of a radome while imaging repeat passes, making variations in performance as a function of antenna scan angle an important consideration.

Ideally, an airborne platform's radome and radar are co-designed to mitigate any deleterious effects by the radome. Even so, platform structural and flight requirements often dictate the mechanical and geometrical design of a radome, leaving limited leeway regarding electrical properties. Furthermore, while the swapping of radar sensors inside existing platforms or pods to meet changing mission demands of customers is often desired, costly and lengthy radome modifications, alterations of platform operational performance, or mission execution delays are not. Unfortunately, radars that rely heavily on phase measurements such as monopulse, interferometric, or CCD systems require the careful design of components that introduce loss and phase variations as a function of the antenna scan angle, such as the radome. Radar performance degradation by the radome needs to be considered part of the mission trade-space as a result.

* amrayna@sandia.gov; phone 1 505 284-3053; fax 1 505 844-0858; www.sandia.gov/radar

The precision-guided munitions literature has analyzed radome effects on monopulse systems for well over half a century.[1-3] The literature emphasizes that radome performance ultimately rests on the radome shape, dimensions, antenna characteristics, and material composition and properties over the desired radar operating parameters. Radome shape impacts the drag experienced by a platform and is often desired to be minimal. Typical radome shapes are: spheres, hemispheres, ogives, ellipses, parabolas, cones, and special mathematical curvatures of the power series, logarithms, or spirals. Radomes often contain a section of different curvature to the main body of the radome known as the fairing, which unites the principal radome shape with the mounting structure of the platform. The fairing usually maintains the same structural and electrical properties of the main body of the radome and is chosen to minimize curvature and slope discontinuities while meeting platform and antenna constraints (i.e. the antenna fitting into the radome via the fairing and the fairing being attachable to the platform opening). All non-spherical shapes have varying degrees of degraded electrical performance. Unfortunately, shapes that yield good electrical performance of the radome often increase drag.

The apparent curvature of a radome seen by the antenna is affected by the radome dimensions and antenna characteristics, which contribute to radar losses and errors. The dimensions of a radome are often summarized by the fineness ratio, F, which is defined as:

$$F = \frac{L_r}{D_r}, \tag{1}$$

where L_r is the length of the radome, and D_r is the diameter of the outside base of the radome. A hemispherical radome shape has a fineness ratio of 0.5. Fineness ratio and the radius of curvature of the radome vertex are more significant for errors as a function of antenna scan angle than the overall shape type. A high ratio implies greater loss tangents, phase shifts, and internal reflections within the radome, which in turn decrease the antenna gain, increase the beamwidth and sidelobe levels, and make performance highly variable versus the antenna scan angle. Changes to the antenna position and size have consequences as well. A spherical radome with a narrow-beam antenna located at the center is ideal for maximum radar performance because the antenna's distance to each portion of the radome is the same, irrespective of angle, and its beam is local to an almost planar area of curvature of the radome wall. However, the antenna size is limited by the available physical space inside the radome and near-field aperture edge effects, which are to be avoided.

A radome's structural properties and materials are of prime importance mechanically to maintain aircraft integrity but cannot be ignored electrically for their influence on radar performance. Material composition and properties affect the heat, pressure, and rain erosion structural response of the radome, which impact radar losses and errors. Electrical properties of interest are the dielectric constant, loss tangent, thickness, and temperature variation of the radome materials. A variety of materials are used for radome design. Typical mechanical and electrical properties of these materials may be found in manufacturer data sheets, materials databases,[4] or the radome literature.[1-2, 5] The control of variability in the radome thickness and material homogeneity or density during manufacturing is crucial to maintaining predictable electrical properties.

Doerry[6], Zebker,[7] and Bickel[8] have detailed many sources of decorrelation by SAR interferometric systems, useful constraints to achieve quality CCD imagery, and metrics to estimate coherence in the presence of error sources. A treatment of radome effects on CCD is lacking in the literature, however. The impact of radome material and wall construction, shape, dimensions, and antenna characteristics on CCD is examined herein for an example Ku-band, fine-resolution radar enclosed in select radomes using electromagnetic simulations. Quantitative and qualitative changes in CCD produced by a radome relative to freespace or changing scan angle are provided. Considerations regarding "adequate" CCD performance are included based on military specifications and professional experience.

This paper is organized as follows. Section 2 describes the methodology and metrics used to evaluate radome CCD performance. Section 3 describes the radome electromagnetic simulations and assumptions. Section 4 details results for select antenna and radome configurations for the example radar. Conclusions are given in Section 5.

2. RADOME DECORRELATION EVALUATION

The total coherence between SAR image pairs can be determined by error sources treated in cascade:[8]

$$\gamma_{\text{TOTAL}} = \gamma_{\text{INTERPOLATION}} \cdot \gamma_{\text{GEOMETRY}} \cdot \gamma_{\text{TEMPORAL}} \cdot \gamma_{\text{SNR}} \cdot \gamma_{\text{IPR}} \cdot \gamma_{\text{MNR}} \cdot \gamma_{\text{POLARIZATION}}, \tag{2}$$

where the differences between the images in interpolation, radar geometry, temporal changes, signal-to-noise ratio (SNR), the impulse response (IPR), multiplicative noise ratio (MNR), and polarization all impact the total coherence. While the first three terms are influenced by variations in the platform flight path or scene, a radome can contribute to

the coherence errors for the latter four terms. For this study, we only examine SNR, IPR, and MNR contributions to coherence, which are defined in Table 1,[8-10] and leave the depolarization contribution of the radome for future work. The subscripted numbers in Table 1 denote the image pass. Parameter definitions and values for the hypothetical Ku-band radar used in this paper are noted in Table 2. Two-way losses through the radome influence the SNR. The one-way loss is given by the reciprocal of the magnitude squared of the normalized transmission, τ, through the radome at the center frequency, f_c, at a specified angle. The impulse response is dependent on the signal processing window applied on receive to the antenna aperture distribution modified by the radome. The impulse response is typically a two-dimensional quantity. However, herein we only examine the principal axis cut in range of the IPR, $x(t)$, which is given by the Fourier transform, $\mathcal{F}$, of the product of the window, W, and normalized complex transmission through the radome over the desired radio-frequency bandwidth at a specified angle. Fine-resolution imaging dictates a small synthetic aperture angle on the order of a few degrees at Ku-band. We assume that the principal axis cut in azimuth of the IPR from antenna scan angle differences through the radome is constant in this paper and leave further investigation for future work. The MNR is defined based on hardware factors such as quantization noise of the analog-to-digital converter (ADC), ambiguities in range and Doppler (AMBR), and integrated sidelobe ratio (ISLR).[10] Of these factors, ISLR will change with radome effects and is also the largest contributor to MNR. ISLR is defined as the integrated sidelobe energy of the impulse response to that of the mainlobe at the first nulls for a specified angle through the radome in this paper. More severe definitions of ISLR may use the 3-dB mainlobe width for normalization.

Table 1. Radome Coherence Budget Equations

Coherence Budget Term	Equation
Signal-to-Noise Ratio (Thermal Noise)	$\gamma_{\mathrm{SNR}} = \sqrt{\frac{\mathrm{SNR}_1}{\mathrm{SNR}_1+1}}\sqrt{\frac{\mathrm{SNR}_2}{\mathrm{SNR}_2+1}}$, $\mathrm{SNR} = \left(\frac{c}{256\pi^3 kT}\right)\left(\frac{\sigma_0}{R^3 v_x \sin\theta_s \cos\psi_s}\right)\left(\frac{P_{avg}{G_A}^2{\lambda_c}^3}{B_T F_N L_{TX}(L_{radome})^2 L_{atmos}}\right)\left(\frac{a_{wr}a_{wa}}{L_r L_a}\right)$, $L_{radome} = \lvert\tau(f_c)\rvert^{-2}$
Impulse Response	$\gamma_{\mathrm{IPR}} = \frac{\langle x_1,x_2\rangle}{\sqrt{\langle x_1,x_1\rangle\langle x_2,x_2\rangle}}$, $\langle x_p, x_q\rangle = \int x_p(t){x_q}^*(t)\,dt$, $x(t) \underset{\mathcal{F}}{\Leftrightarrow} \tau(f)W(f)$
Multiplicative Noise Ratio (Uniform clutter)	$\gamma_{\mathrm{MNR}} = \sqrt{\frac{1}{\mathrm{MNR}_1+1}}\sqrt{\frac{1}{\mathrm{MNR}_2+1}}$, $\mathrm{MNR} = \mathrm{QNR} + \mathrm{AMBR} + \mathrm{ISLR}$, $\mathrm{ISLR} = \int_{sidelobes} x(t)\,dt \Big/ \int_{mainlobe} x(t)\,dt$
Radome Total	$\gamma_{\mathrm{RADOME}} = \gamma_{\mathrm{SNR}} \cdot \gamma_{\mathrm{IPR}} \cdot \gamma_{\mathrm{MNR}}$

The coherence budget contribution of a radome is evaluated by computing the SNR, IPR, MNR, and total radome decorrelation three different ways in this paper. First, a severe case of a hypothetical freespace image (i.e. one with the radome off) is correlated against an image with the radome on, as a function of antenna scan angle. Second, a more realistic, severe case is examined due to two images with the radome on and a platform (and radome) yaw angle difference of 15 degrees from the antenna scan angle in the second pass. The chosen yaw angle is close to the 90% cumulative probability due to radiosonde monthly average wind characteristics worldwide from 1940 onwards at the example platform parameters.[12] Lastly, a more benign decorrelation case is examined of two images with the radome on, where the antenna is at broadside only and yaw angle differences of 0 to +/-45 degrees occur in the second pass. (The maximum yaw angle from radiosonde mean monthly wind characteristics at the noted platform parameters is close to 45 degrees.) Mean total coherence values over all radome, yaw, or antenna scan angles configurations are used to summarize results.

To compare radome performance objectively using our evaluation methods, we incorporate military requirements and institutional experience. Radomes may be described by their grade, class, type, and style per military specification MIL-R-7705B.[13] Grades determine whether damage to the radome can impact platform airworthiness, personnel safety, or the antenna. Classes account for the radar platform. Types identify the required radome fractional bandwidth, frequency, or

functionality. Styles define the radome thickness, fractional bandwidth, and construction characteristics. Radome constructions are either monolithic (i.e. a single solid) or a sandwich (i.e. layers of alternating material densities and thicknesses) involving resins, plastics, or glass. Sandwich style radomes are more broadband than monolithic radomes and have higher strength-to-weight ratios. An airborne, Ku-band, fine resolution SAR or CCD system with a fractional bandwidth between 5 and 20%, depending on squint angle and resolution,[14] is considered a primary or secondary radome (Grade A or B) for a flight vehicle (Class I) with directional guidance or broadband characteristics (Type II or V) and A-sandwich or multi-layer sandwich construction (Style c or d). All other type and style combinations of radomes are not designed for aircraft at Ku-band due to structural, fractional bandwidth, or frequency limitations. Multilayer (Style d) radomes are more broadband, at the expense of increased insertion phase delay (IPD) at high grazing angles.

Table 2. Example Radar Parameters

Parameter	Symbol	Units	Value
Speed of Light	c	m/s	299792458
Boltzmann's Constant	k	J/K	1.38×10^{-23}
Standard Temperature	T	K	290
Average Power	P_{avg}	W	100
Altitude	AGL	kft	20
Platform Velocity	v_x	m/s	150
Grazing Angle (Broadside)	ψ_B	°	[10:65]
Squint Angle	θ_s	°	[45:135]
Nominal Grazing Angle (Squint)	ψ_s	°	$\tan^{-1}(\tan\psi_B \sin\theta_s)$
Clutter Reflectivity[11] (Dry Soil, VV or HH vs. $\boldsymbol{\psi_s}$)	σ_0	dB	[-18.1:-4.9] or [-20.9:-4.9]
Platform Yaw Angle	θ_{yaw}	°	[0:45]
Slant Range	R	m	$AGL\,(0.3048)/\sin\psi_s$
Antenna Gain	G_A	dBi	30
Center Wavelength	λ_c	m	0.02
Bandwidth at 4" Range Resolution	B_T	Hz	1.744×10^9
Noise Figure	F_N	dB	4.5
Radar Transmitter to Antenna Port Loss	L_{TX}	dB	2
Atmospheric 2-Way Loss (Clear Air, 50% Humidity)	L_{atmos}	dB	$0.00003R$
Range and Azimuth Window	W_r, W_a	-	Taylor, -35 dB Sidelobes, $\bar{n}$=4
Range and Azimuth Window Factor	a_{wr}, a_{wa}	-	1.1822
Range and Azimuth Losses	L_r, L_a	dB	1
Quantization Noise for 8-bit ADC (-5dB/bit)	QNR	dB	-40

Detailed requirements for radomes vary by application, as well as radome type, class, and style. Performance requirements noted for a Type V radome in MIL-R-7705B[13] or gathered from professional experience with SAR systems indicate that the average and minimum transmission should be no worse than 80 and 70%, respectively; reflection should be below 2%; the dielectric constant for airborne systems should be below 1.5; a change in the antenna mainlobe 3dB beamwidth or amplitude ripple within this width should be no worse than 10% and 0.2 dB, respectively; the impulse response sidelobe level should not increase beyond 2 dB; and the insertion phase delay should be no worse than 3 degrees. Type II radomes have stricter requirements for certain metrics such as 85 and 75% for the average and minimum transmission, respectively; 5% and 0 dB for antenna 3dB mainlobe beamwidth changes and amplitude ripple; and 1.5 degrees for the maximum IPD. Microwave and millimeter wave frequency radomes will also generally observe loss tangents below 0.01.[1]

CCD expectations using these requirements for our radar point design in Table 2 and a radome on versus off repeat-pass scenario indicate the following. The SNR decorrelation should be above 0.951 for vertical polarization and 0.933 for horizontal polarization to achieve the greater than 70% transmission requirement. IPR decorrelation should be above 0.998, assuming a linear trend in transmission from 70 to 100% and insertion phase delay from -3 to 3 degrees, to fulfill the 70% transmission and 3-degree IPD requirements. Results may be far worse if the parameters vary quickly and non-linearly, with the worst case being completely random values within the established bounds. MNR decorrelation should be above 0.998 to meet the 2 dB bound on the ISLR of the impulse response. In total, the radome decorrelation should be no worse than 0.947 for vertical polarization, and 0.929 for horizontal polarization. We leverage all of these requirements to gauge radome-antenna configuration performance in our results.

3. RADOME MODELING FOR CCD PERFORMANCE PREDICTION

Electromagnetic modeling approaches for performance prediction of a radome are typically selected based on the radome size and shape, the antenna size and location within the radome, and the degree of performance prediction accuracy needed or desired for the available time and resources. Kozakoff[1] and Tice[2] detail several techniques for analyzing radome-enclosed antenna performance, their benefits, and disadvantages. While accurate and general performance prediction methods for electrically small radomes are quite specialized and computationally expensive to account for near-field effects, large radomes can be simply and quickly analyzed using ray-tracing to find reasonable asymptotic approximations. A radome is considered electrically large in the far-field sense if: the antenna aperture diameter equals or exceeds 10 wavelengths; the separation distance between the scanning antenna edges and radome inner wall is at least a wavelength; and the curvature of the wall is less than a wavelength.[2]

To determine the normalized complex transmission through the radome at a given angle and frequency for CCD performance evaluation, the transmit-mode, geometrical optics, ray-tracing method outlined by Kozakoff is used in this paper for electrically large radomes.[1] Geometrical optics ray-tracing treats electromagnetic propagation through the radome as a light-like plane wave field, where a surface is lit or unlit by the rays forming the field, and Snell's Law applies for refraction and reflection. The phase of the field of each ray is determined separately from its amplitude, which is found by accounting for intensity variations along its path independently of other rays. Transmit mode ray-tracing launches uniformly spaced rays from the antenna aperture toward the radome, which are traced to intercept points on the radome and through the wall based on the angle of incidence to find resulting transmission coefficients. The Fourier transform of the transmission-coefficient-modified antenna aperture distribution beyond the wall yields the modified far-field antenna pattern. Antenna polarization is included in the transmission coefficient determination through the radome. The normalized complex transmission through the radome at each angle and frequency is found by normalizing the modified antenna aperture distribution sum through the radome to the aperture distribution sum without the radome (i.e. the antenna alone).

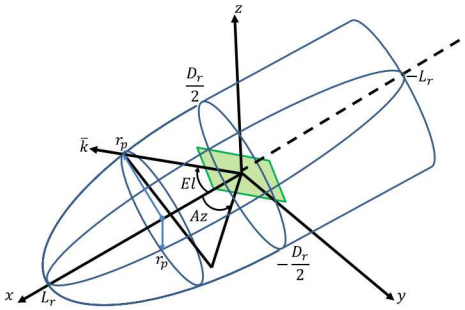

Figure 1. Radome-Antenna Coordinate System

We select Kozakoff's method for reasons of simplicity, speed, and reasonable accuracy on a personal computer to provide an efficient and acceptable engineering assessment of radome errors and intuition about radome and antenna design parameters on a CCD system. To reduce computation time, Kozakoff treats the radome as a two-dimensional body-of-revolution that leverages axial symmetry of the radome about the nose of the aircraft (i.e. 0 degrees azimuth and elevation) to expedite the ray-tracing solution and circumvent the need for a full three-dimensional solver. The radome and antenna coordinate system is shown in Figure 1. The radius perpendicular to the point along the x-axis of revolution, r_p, depends on the y- and z-coordinate along the xy- or xz-plane and has an instantaneous slope, dr_p/dx. The yz-plane cross-section of the radome at some specific point along x, is a circle of radius r_p. Analytical equations for the radome shape and slope are further used to simplify computations regarding the radome wall curvature and ray-tracing to the wall. The definitions utilized in this paper are shown in Table 3.[1-2] All non-spherical shapes have a cylindrical fairing as defined in the table to allow for backward squinting of the antenna devoid of a free-space discontinuity at the radome base, which would not occur on a real platform. Locally planar radome walls, with parallel inner and outer boundaries, homogeneous wall materials of constant thicknesses, and a lack of multiple reflections are also assumed at ray hit points.

Modeling errors in the accurate determination of radome performance compared with chamber and field measurements usually originate from the: antenna aperture; dielectric density, thickness, or anisotropic variations in the radome wall with frequency; overall radome shape thickness and curvature; internal reflections; conducting radome or radar components such as rain erosion tips, lightening arrestors, bulkhead plates, gimbals, etc; and external obstructions of the

platform.[1] The most significant error sources are from radome wall design tolerances, diffraction from a thick and sharp wall curvature or rain erosion tips, and internal reflections that enter the backlobe of the antenna from non-absorbing, planar radar components. External obstructions by the wing or underside of the aircraft may also impact the radiation pattern through diffraction and reflection.[2]

Table 3. Example Radome Shape and Slope Analytical Equations

Shape	Curvature	Slope of Curvature
Power Series ($x \in [0, L_r]$) Cone: $m = 1$, Parabola: $m = 0.5$	$r_p = \frac{D_r}{2}\left(1 - \frac{x}{L_r}\right)^m$	$\frac{dr_p}{dx} = -\frac{mD_r}{2L_r}\left(1 - \frac{x}{L_r}\right)^{m-1}$
Ellipse ($x \in [0, L_r]$) Hemisphere: $F = 0.5$	$r_p = \frac{D_r}{2}\left[1 - \left(\frac{x}{L_r}\right)^2\right]^{0.5}$	$\frac{dr_p}{dx} = -\frac{xD_r}{2{L_r}^2}\left[1 - \left(\frac{x}{L_r}\right)^2\right]^{-0.5}$
Ogive ($x \in [0, L_r]$) Hemisphere: $F = 0.5$	$r_p = [R^2 - x^2]^{0.5} - \mathrm{B}$ $(R = \frac{{L_r}^2}{D_r} + \frac{D_r}{4}, B = \frac{{L_r}^2}{D_r} - \frac{D_r}{4})$	$\frac{dr_p}{dx} = -x[R^2 - x^2]^{-0.5}$
Sphere ($x \in [-L_r, L_r]$)	$r_p = \left[{L_r}^2 - x^2\right]^{0.5}$	$\frac{dr_p}{dx} = -x\left[{L_r}^2 - x^2\right]^{-0.5}$
Cylindrical Fairing ($x \in [-2L_r, 0)$)	$r_p = \frac{D_r}{2}$	$\frac{dr_p}{dx} = 0$

While we do not concern ourselves with the measurement fidelity of our simulations in this paper and leave this for future work, we do attempt to control modeling error sources. For example, the Ku-band radar frequency is not subject to material anisotropy; conducting radar or radome components do not exist except for the antenna; and the radome shape, size, and wall electrical properties, and antenna location, size, and aperture distribution, are all pre-defined. Although statistical variations in the radome wall may occur in practice, they may be measured or bounded by typical error tolerances for the manufacturing process. We examine cases of wall error tolerance effects in Section 4. Per the literature, secondary or multi-bounce reflections from a radome wall are miniscule and ignored.[1] While initial reflections may reach the antenna and be absorbed according to the aperture distribution, which may have a taper to dampen the energy at the edges, these reflections are ignored in this paper. Military specifications dictate reflections should be below 2% and thus unlikely to dominate transmission loss trends. If a best-case error from transmission-only losses is poor, internal reflections will certainly only make results even less acceptable. Lastly, no external effects are considered, since they encompass a larger system design problem than the mere radome. (However, design rules of thumb can help avoid external effects by ensuring the centerline and rays from the edges of the antenna at its location within the radome are, respectively, 5 degrees and 1.5 inches clear of any platform obstructions for any operational incidence angle.[2])

Table 4. Example Radome Style and Electrical Properties

Radome	Material Layers	Dielectric (ε_r')	Loss Tangent (tan δ)	Thickness (m)
A-Sandwich	E-Glass Skins/Korex Core	4.1/1.1	0.004/0.005	0.0055/0.0125
Monolithic	E-Glass	4.1	0.004	0.022

We evaluate the following radome-antenna system configurations to denote radome material, wall construction, shape, dimensions, and antenna characteristic effects. An A-sandwich radome wall defined in Table 4 is the default design. To illustrate the influence of wavelength on radome design, we additionally examine a Ku-band, fine resolution radar enclosed in the fiberglass monolithic thin-wall radome in Table 4 meant for a UHF-band radar with a center frequency of 0.3 GHz and bandwidth of 0.175 GHz. We also examine manufacturing tolerance changes to the A-sandwich layer thickness by 1 mm and dielectric properties by 0.1+j0.001. The change in thickness is a reasonable error for wet layup manufacturing per 11-mm ply.[1] The dielectric change is an assumption based on observed fluctuations in quoted manufacturer specifications for similar materials. The default radome is an ellipse 24 inches long and wide (i.e. F=1). Spherical, hemispherical, parabolic, ogive, and conical radome shapes of similar dimensions are additionally investigated to show the influence of radome shape. An ellipse with a base diameter of 16 inches (i.e. F=1.5) is also examined for shape curvature effects. The default antenna is a vertically-polarized, 6-inch square, Ku-band, planar phased array with a uniform rectangular aperture illumination located at the center base of the radome shape. The antenna is assumed to be gimbaled with negligible offsets. Changes to horizontal polarization; a 14-inch size in azimuth;

and a -30 dB sidelobe, $\bar{n} = 4$, Taylor aperture taper are examined for the more severe F=1.5 ellipse. An antenna shift 2-inches back from center is included for evaluation using a spherical radome as well.

4. RESULTS AND DISCUSSION

We proceed to show effects produced by the properties of the radome wall composition, shape, fineness ratio, and antenna size, location, polarization, and aperture taper next. First, we examine radome wall composition effects. Figure 2 shows the radome wall transmission, reflection, and insertion phase delay difference of the transverse electric (TE) and magnetic (TM) fields versus frequency and ray angle of incidence to the radome wall for the A-sandwich at Ku-band and the monolithic UHF design at both the design frequency of UHF and at Ku-band. (Energy that hits a radome wall at normal incidence does not generally have both TE and TM modes, but oblique incidence will cause this change. The overall complex radome transmission at an antenna scan angle will be the vector sum of the contributions of these modes in the plane of incidence that are aligned with the antenna polarization over the entire aperture distribution.) Ideally, a radome wall design should demonstrate a constant response over the frequency bandwidth, with minimal deviations over ray incidence angles, and losses abiding by military specifications.

The data in Figure 2 shows that none of the wall designs are ideal, particularly at severely oblique angles of incidence to the normal of the radome wall. If we ignore performance at these incidence angles for a moment, the A-sandwich generally meets requirements but varies with frequency to the extent that performance is border-line at the upper parts of the bandwidth. On the other hand, the monolithic UHF system radome has been well-designed to minimizes dispersion at a given incidence angle and meet radome requirements over the desired bandwidth. A Ku-band system forced to use this radome not only encompasses an entirely different and larger bandwidth, but the characteristics are not well-behaved (i.e. dispersion is severe and requirements in transmission and reflection are not met over many incidence angles that include the normal to the surface). If the radome wall were any thicker, the Ku-band system would show severe oscillatory behavior with frequency. In short, matching the design frequency and bandwidth of the radome wall to those of the desired radar matters. A good radome wall design at one band does not translate into a good radome wall design for a radar at another center frequency, bandwidth, or frequency band.

As for wall composition thickness and dielectric changes from manufacturing error tolerances, Figure 3 shows the A-sandwich radome wall TE transmission, TE reflection, and insertion phase delay difference versus frequency and ray incidence angle. (TM modes are not shown in the interest of space but have similar trends as TE modes.) Errors in skin layers of the radome are more pronounced than those of the core, since the layer is thinner and more lossy. In particular, the wall performance at angles near the normal in the upper portion of the frequency bandwidth cease to comply with military requirements. Compound errors would alter response characteristics further. Hence, measuring and statistically bounding layer manufacturing tolerances is an important consideration for understanding and controlling wall performance fluctuations. We shall see more evidence of wavelength and manufacturing error wall composition effects when evaluating CCD performance later.

However, now we address the likelihood of whether large performance degradation can be expected by severely oblique ray incidence angle behavior for a given radome shape, fineness ratio, and antenna configuration, which we have been temporarily ignoring in the above discussions. The cumulative probability of each ray in our electromagnetic simulation hitting a given angle of incidence to the wall for various configurations over all antenna scan angles from 0 to 135 degrees is shown in Figure 4a). All rays from a spherical radome occur very close to normal incidence (i.e. below 10 degrees for our parameters), which is where the wall designs show the best performance. Antenna positions off-center from the sphere (or away from the focal point of the given shape) will cause larger incidence angles to occur. Hemispherical radomes will perform like a sphere but with some larger incidence angles due to the discontinuity between the radome and fairing. Thus minimizing this discontinuity or avoiding its illumination by the radar is key. Other shapes of similar fineness ratio show a higher probability of having large incidence angles to that of the hemisphere, and this probability increases with increasing fineness ratio, as shown by the 1 and 1.5 fineness ratio ellipse results. Therefore, non-spherical shapes will tend to have worse performance losses through the radome wall. Lastly, larger antenna sizes within the radome (i.e. a narrower beam) will generally hit the wall at incidence angles closer to the normal more consistently, providing better performance, except in certain cases where rays from the edges of the antenna may hit at more oblique angles than those of a smaller antenna. Additional caution should be taken to avoid near-field effects from illumination of the radome by the edges of a large antenna. In short, a spherical radome, with a centered and large antenna, will generally avoid oblique incidence angles that generate poor performance. Other shapes, fineness ratios, or antenna configurations should be studied carefully for expected wall performance.

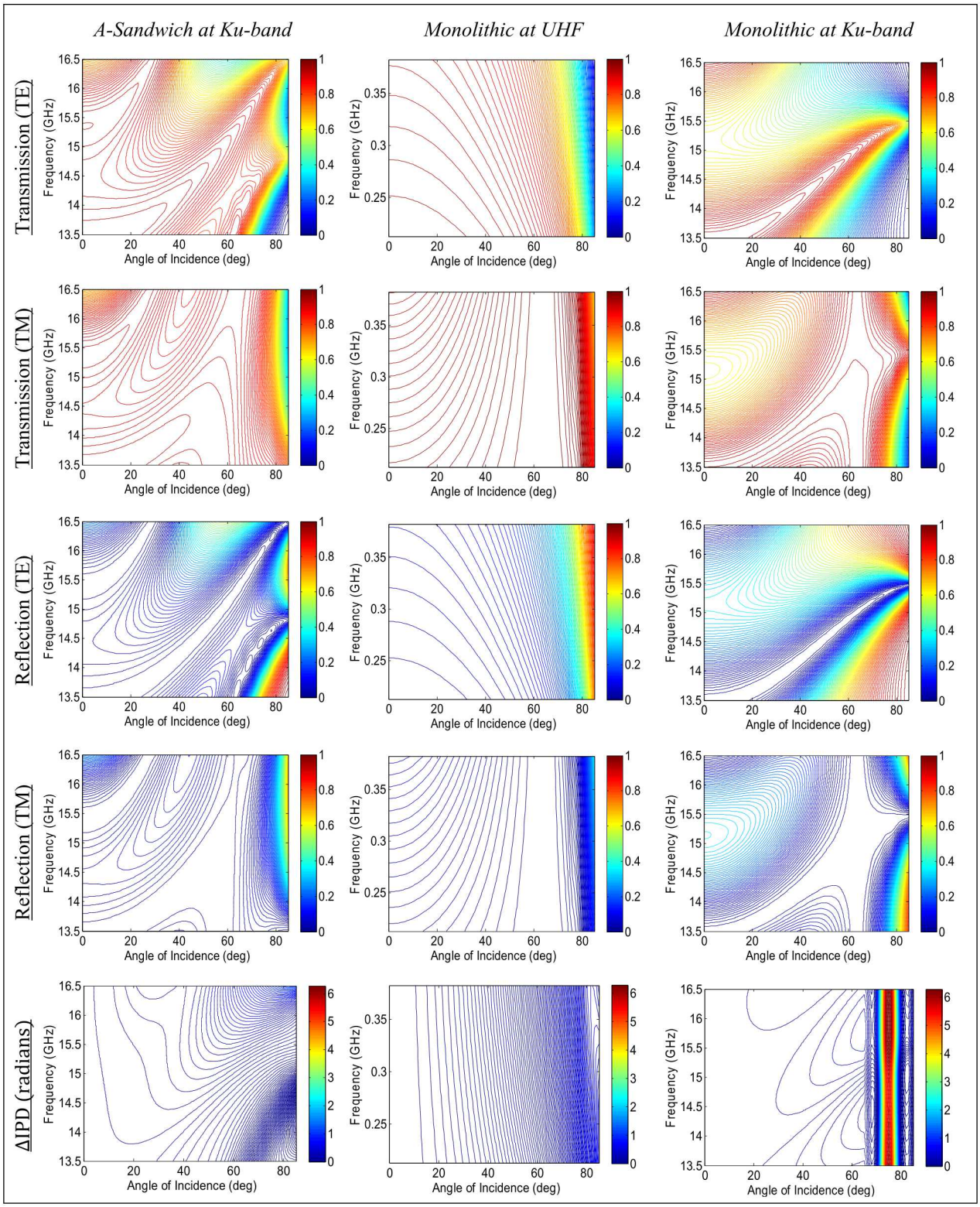

Figure 2. Radome Wall Transmission, Reflection, and Insertion Phase Delay Difference Comparison vs. Frequency and Ray Angle of Incidence

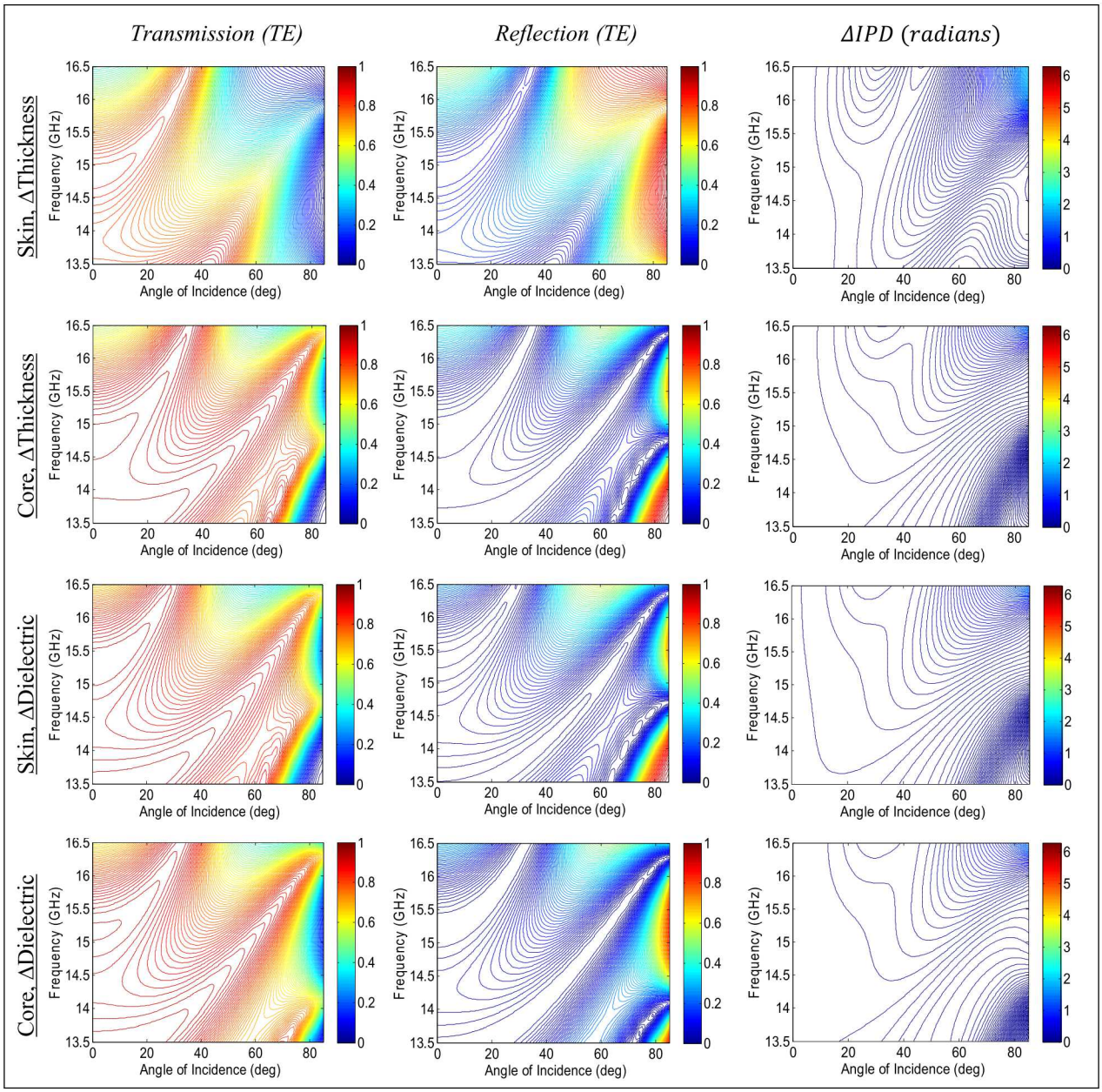

Figure 3. A-sandwich Radome Wall TE Transmission, TE Reflection, and Insertion Phase Delay Difference Layer Manufacturing Effects vs. Frequency and Ray Angle of Incidence for 1 mm Thickness and 0.1+j0.001 Dielectric Errors

Transitioning to a higher, system-level of detail, Figure 5, Figure 6, and Figure 7, show the overall transmission, insertion phase delay, and impulse response of various radome and antenna configurations versus scan angle. Figure 4b) shows the ideal impulse response of a -35 dB Taylor window of $\bar{n} = 4$ for impulse response comparison purposes. The red lines and markers indicate a worst case bound on performance defined by a 10% mainlobe broadening at the 3-dB point, -18-dB mainlobe broadening 3 times beyond the nominal ideal resolution, and an envelope decay of approximately a power of 2 for near-in sidelobes and linear decay for far-out sidelobes. The characteristics of the spherical radome in Figure 5 are uniform with angle as expected, with slight dispersion as was evident in the wall characteristics for the A-sandwich. Thus the impulse response greatly resembles that of the ideal window. The subtle change in the antenna placement 2-inches away from the center results in some, albeit small, angular variations. Although this particularly small change does not result in a severe degradation of the impulse response, accurate antenna placement remains a general concern for larger and possibly asymmetric deviations along multiple axes.

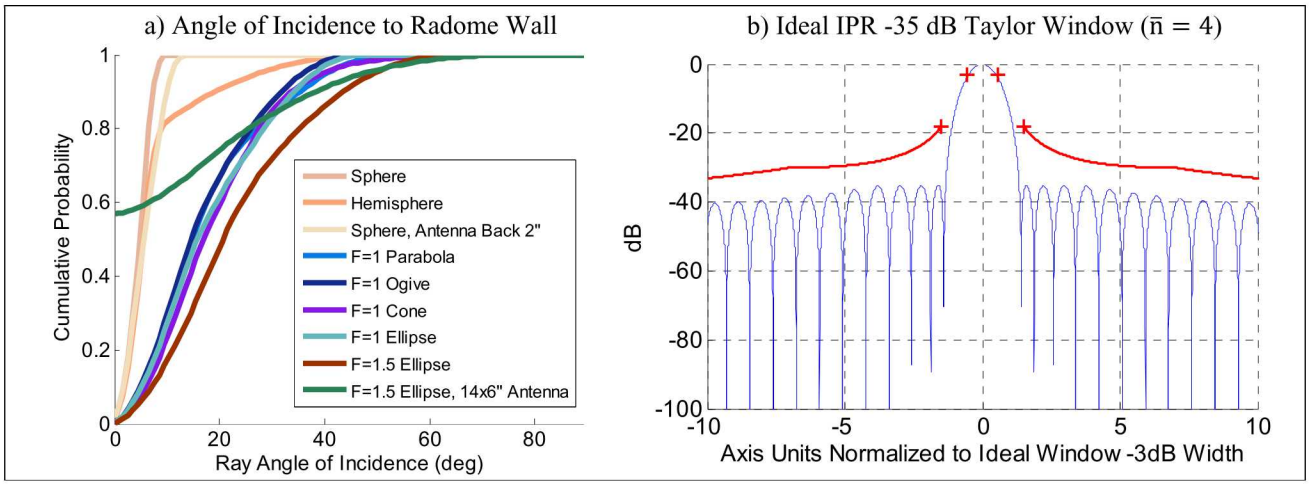

Figure 4. Characteristics of a) Angle of Incidence to Radome Wall vs. Radome, and b) Ideal Impulse Response

Differences between radome shapes with a fineness ratio of 1 are shown in Figure 6 (except for the hemisphere whose fineness ratio is always 0.5). The hemisphere is similar in angular uniformity and dispersion performance to the sphere, except at and beyond the fairing juncture where it does not meet requirements. The insertion phase delay is capped at +/- 5 degrees for display purposes, but might exceed this amount beyond the radome azimuth angle of 90 degrees. Consequently, the impulse response for the hemisphere includes some elevated sidelobe, broadened mainlobe, reduced peak level, and asymmetric characteristics compared with the ideal case. Results vary with angle and frequency for the other shapes (i.e. the ellipse, parabola, ogive, and cone), producing altered impulse responses from the ideal case. The cone demonstrates the worst performance, particularly near the nose of the radome, and has an impulse response at certain scan angles that exceed our performance bounds. The plunge in performance near the nose of the cone is a known characteristic exhibited by the shape due to lensing effects.[2] It is important to keep in mind that although for SAR systems, squint angles of the antenna are generally kept in the region of 45 to 135 degrees, the yaw of the platform and radome can cause a radar system to look through these undesired angles at the radome nose.

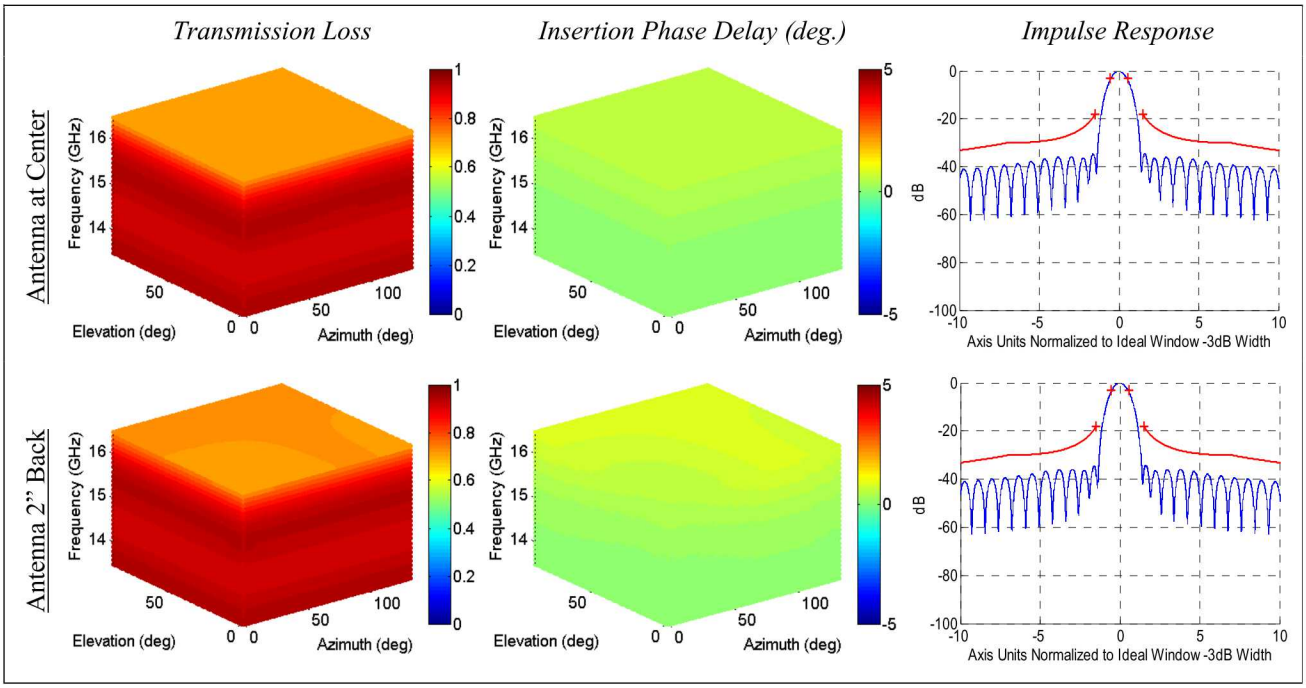

Figure 5. Transmission Loss, Insertion Phase Delay, and Impulse Response vs. Antenna Location (Spherical Radome)

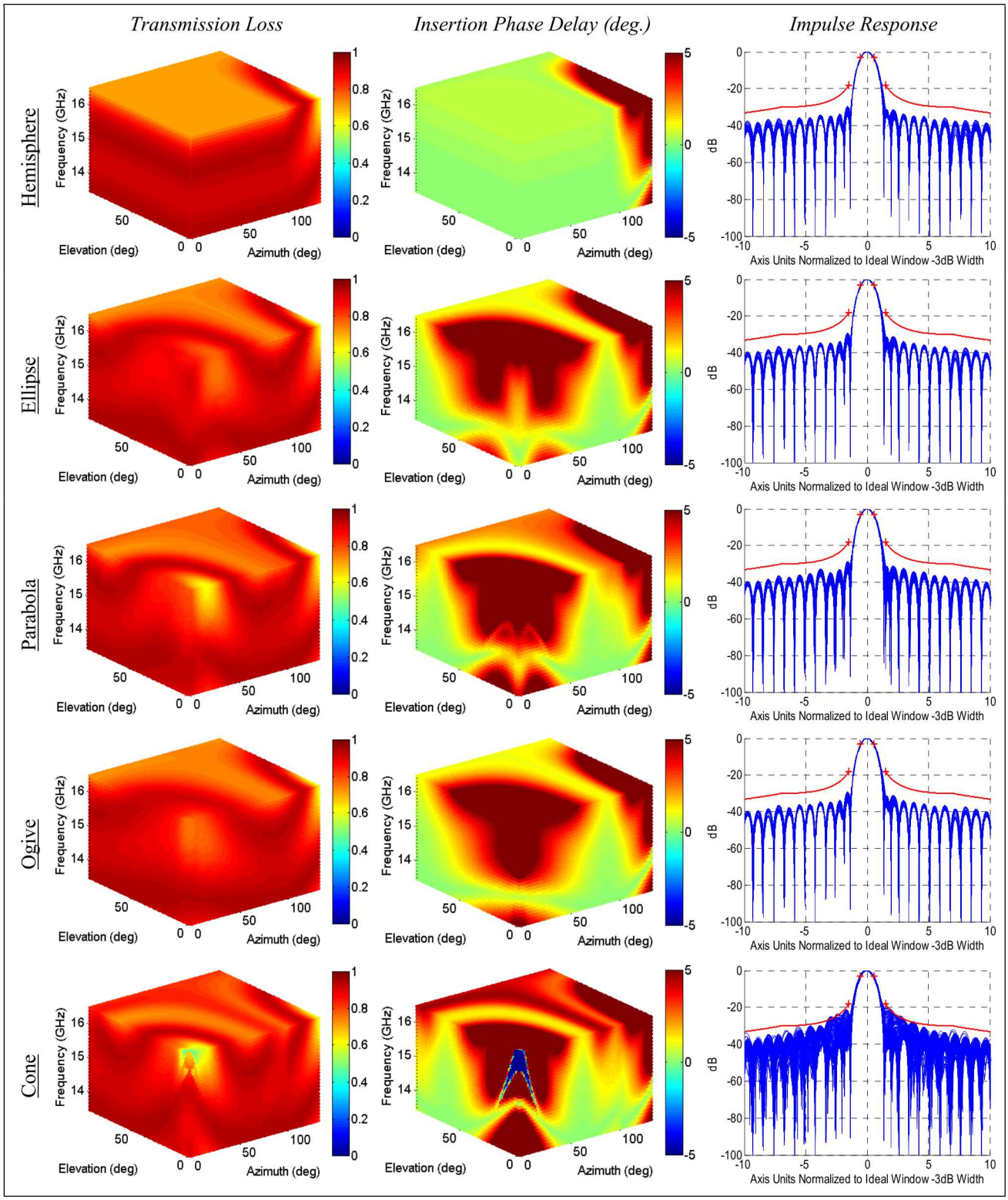

Figure 6. Transmission Loss, Insertion Phase Delay, and Impulse Response vs. Radome Shape (F=1, except Hemisphere)

Differences produced by an increased fineness ratio to 1.5 in the ellipse, compared with the prior figure, and several changes in antenna characteristics (i.e. aperture taper, polarization, size) and radome wall composition are shown in Figure 7. As with the ray angle of incidence discussion, the fineness ratio change in the ellipse degrades performance, causing the ellipse to fail requirements at a greater number of scan angles. Aperture taper does not make a stark change in performance, nor does a polarization change from vertical to horizontal. The angles at which degradation occurs do swap axes from azimuth to elevation, however, because of the polarization change and the symmetric antenna size. This effect is most evident at the radome nose. The increased antenna size improves impulse response performance for sidelobe levels away from the mainlobe but not those close to it, and the transmission and insertion phase delay variations are worse. The monolithic UHF radome design at Ku-band performs the worst of all shown examples in terms of transmission loss and IPR, which confirms results foreshadowed by the monolithic wall performance at Ku-band.

The aforementioned radome effects ultimately manifest as the example radome coherence characteristics as a function of antenna scan or yaw angle shown in Figure 8. The results shown are for a spherical A-sandwich radome with the antenna at the center, but all other configurations we have been examining have similar behavior with only subtle visual distinctions that are not worth illustrating. The coherence for our chosen radar example is dominated by the signal-to-noise ratio contribution. Because we have kept the altitude fixed in our analysis, longer ranges where thermal noise will dominate occur at lower grazing angles. These are therefore, the angles where our coherence is lowest. Changes in the yaw angle of the radome on the second pass slightly change the characteristics of the coherence with angle. Fortunately, the decorrelation caused by the radome is small for most angles in our parameter space for all three of our evaluation methods.

The mean coherence over the antenna scan angles of interest for all radome configurations discussed is shown in Table 5. The SNR, IPR, and MNR contributions to the case where the radome is on in one pass and hypothetically off in the second pass are also shown. While the SNR, IPR, and MNR affect coherence minimally, the SNR term is certainly the worst factor for our chosen radar example for any configuration. Some caution is necessary regarding the interpretation of the IPR contribution to coherence because its measure of decorrelation depends on the similarity, and not the quality, of the impulse responses being compared between passes. Thus poor, but similar, impulse responses can yield good coherence. However, poor impulse responses lead to artifacts, loss of resolution, loss of statistical independence in the effective number of looks, and decreased detection in SAR and CCD imagery overall, which are clearly undesired and unaccounted by the coherence metric alone. Thus, the best CCD radar system has good-quality and similar impulse responses across radome scan angles, which we have seen to be false for non-spherical shapes. Lastly, Table 5 shows that a broadside-only imaging configuration, regardless of whether the radome has a yaw angle from 0 to 45 degrees produces the best coherence performance, while squinting causes more degradation in the signal-to-noise contribution. Large squint angles can further cause decorrelation effects related to geometry and registration which make them additionally undesirable for CCD.[6] Although the case of the radome being off on the second pass is much easier to realize in theory, the worst case coherence evaluation method is that of the 15-degree yaw angle shift over all squint angles and may be the most realistic way to determine radome coherence performance.

In general, the trends for all three coherence evaluation methods are similar across the various radome and antenna configurations. As one might expect, the sphere has the least decorrelation. Changes to the antenna location 2-inches back from the center of the sphere cause negligible change in coherence, though more severe shifts may not be so benign. Errors in the layers of the A-sandwich design due to manufacturing tolerances can vary the coherence. The skins of the radome are more susceptible than the core due to the fact that the layer thickness is smaller and dielectric properties are worse in relationship to the same magnitude errors. The hemisphere performs slightly worse than the sphere due to the fairing. Other shapes with a fineness ratio of 1 also perform slightly worse. A change in the fineness ratio of the ellipse to 1.5 negligibly decreases performance, though a sharper curvature may prove otherwise. Also, a change in the aperture taper of the ellipse to the Taylor window provides negligible improvement. Horizontal polarization causes the coherence to drop due to the clutter reflectivity being lower than vertical polarization for dry soil, which affects the signal-to-noise ratio, rather than a discrepancy attributable to the radome. Changes in the antenna size create negligible impact to the coherence for our chosen parameters. Finally, once again, the monolithic UHF radome design used at Ku-band is the overall worst-performing radome configuration, regardless of the coherence repeat-pass method used for evaluation. A maximum decrease in coherence of about 0.02 versus the A-sandwich with values around 0.96 is noted. Of all the radome-antenna configurations, only this one fails our radome coherence budget requirement of 0.947 based on the established military and institutional specifications for the radome off repeat-pass.

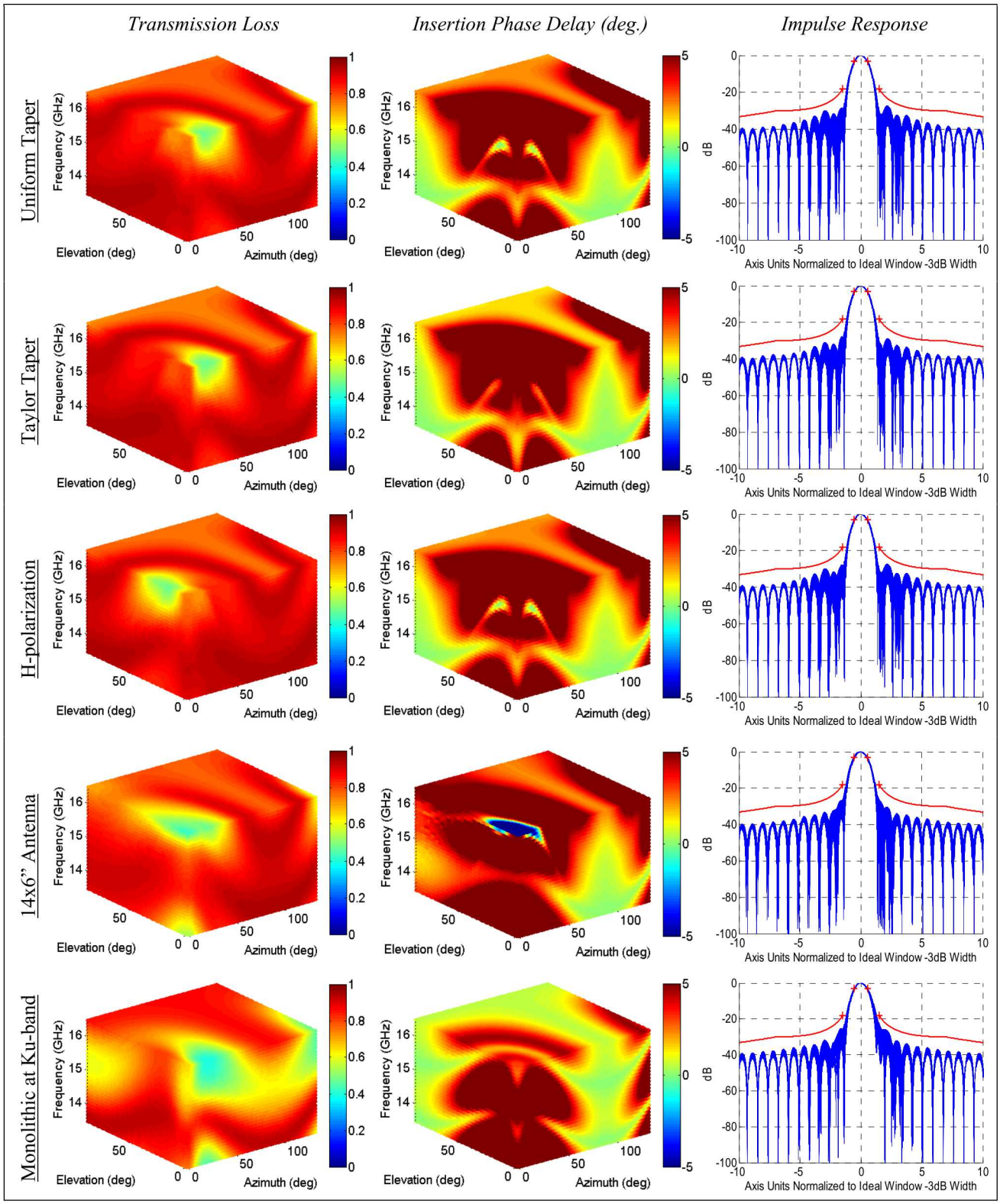

Figure 7. Transmission Loss, Insertion Phase Delay, and Impulse Response vs. Antenna and Radome Style (Ellipse, F=1.5)

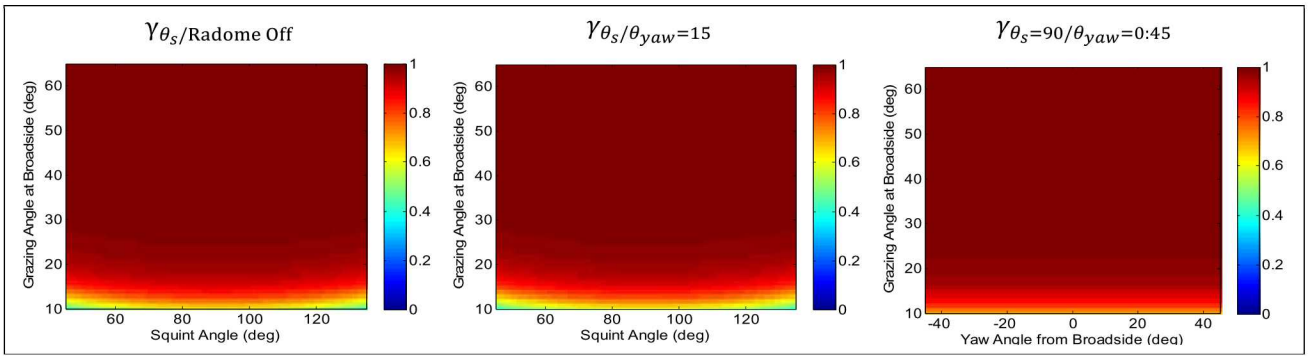

Figure 8. Spherical Radome Coherence with Antenna Scan Angle

Although performance distinctions between one radome configuration and another may seem insignificant, if a radar system does not minimize all decorrelation contributions from itself, it has less ability to detect temporal decorrelation from the desired scene. A typical CCD radar system should strive for a coherence budget above 0.9.[6] Since the radome coherence budget is a part of the larger system coherence budget, if more decorrelation must be budgeted for the radome, then less is available for geometry, registration, interpolation, and other radar system concerns that accumulate as a cascaded product of errors. Thus, the amount of tolerable radome decorrelation or required modifications to improve radome coherence need to be a part of the radar and mission trade space decision process, which has been generally ignored to date.

Table 5. Radome-Antenna System Mean Coherence for Various Radome-Antenna Configurations

Radome-Antenna System	γ_{SNR}	γ_{IPR}	γ_{MNR}	$\gamma_{\theta_s/\text{Radome Off}}$	$\gamma_{\theta_s/\theta_{yaw}=15}$	$\gamma_{\theta_s=90/\theta_{yaw}=0:45}$
Sphere	0.962	0.998	1.000	**0.960**	**0.958**	**0.974**
Sphere, Antenna Back 2”	0.961	0.998	1.000	**0.960**	**0.958**	**0.974**
Sphere, 1mm Skin Error	0.958	0.998	0.999	**0.955**	**0.951**	**0.969**
Sphere, 1mm Core Error	0.962	0.998	0.999	**0.959**	**0.958**	**0.974**
Sphere, 0.1+j0.001 Skin Error	0.961	0.998	1.000	**0.959**	**0.957**	**0.973**
Sphere, 0.1+j0.001 Core Error	0.961	0.998	1.000	**0.960**	**0.958**	**0.974**
Hemisphere	0.961	0.998	1.000	**0.959**	**0.956**	**0.973**
Ellipse, F=1	0.960	0.998	1.000	**0.958**	**0.954**	**0.972**
Parabola, F=1	0.960	0.998	1.000	**0.958**	**0.955**	**0.972**
Ogive, F=1	0.960	0.998	1.000	**0.958**	**0.955**	**0.972**
Cone, F=1	0.960	0.998	1.000	**0.958**	**0.955**	**0.972**
Ellipse, F=1.5	0.960	0.998	1.000	**0.958**	**0.954**	**0.972**
Ellipse, F=1.5, Taylor Taper	0.960	0.998	1.000	**0.958**	**0.954**	**0.972**
Ellipse, F=1.5, H-polarization	0.939	0.998	1.000	**0.937**	**0.933**	**0.957**
Ellipse, F=1.5, 14x6” Antenna	0.960	0.998	1.000	**0.958**	**0.954**	**0.972**
Ellipse, F=1.5, Monolithic	0.947	0.997	0.998	**0.942**	**0.929**	**0.952**

5. CONCLUSIONS

Coherent change detection (CCD) estimates subtle phase differences between repeat-pass synthetic aperture radar (SAR) images of a scene. A CCD radar system’s goal is to minimize all decorrelation contributions from itself in order to have the maximum ability to highlight temporal decorrelation from the desired scene. Radomes, no matter how well-designed electrically, impact the radiation pattern of an antenna. This paper has addressed CCD performance with respect to radome material construction, shape, dimensions, and antenna characteristics. Contributors to coherence degradation such as transmission loss, insertion phase delay, and ultimately the radar impulse response have been qualitatively examined for various radome-antenna configurations of a specific radar point-design, and the coherence of the radomes have been quantified through geometrical optics electromagnetic simulations in order to understand their effects. Results have been further compared to expected military or institutional imaging radar specifications.

We have come to the following conclusions for radome effects on CCD. Manufacturing tolerances in layer thickness and electrical properties should be statistically measured and bounded as they can increase the decorrelation of the radome, depending on their severity, particularly for thin layers with highly lossy materials. The fineness ratio, shape, and antenna location within a radome matter in determining the radome CCD performance. A spherical radome with the antenna at the center is always preferable for its uniform angular characteristics. Antenna locations away from the center of a sphere, however, may alter the uniform angular performance of the shape. A hemispherical radome with fairing will perform much like a sphere, so long as antenna pointing angles are not near the juncture between the different curved surfaces. Ellipse, parabola, ogive, and cone shapes perform more poorly near the nose or fairing and for higher fineness ratios (i.e. more streamlined, sharper curvatures). An aperture taper versus a uniform illumination by the antenna may only mildly improve coherence. Coherence between vertical and horizontal polarizations may be different due to the imaging scene reflectivity response, but not due to the radome (unless the materials are anisotropic or depolarization is examined). Larger, narrower beam, antenna sizes provide negligible impact to coherence. Independent motion of the radome with the platform versus the radar antenna pointing angle may cause uncontrolled and difficult to compensate transitions into regions of highly variable losses such as the nose for non-spherical radomes. Radome wall designs at frequency bands that are poorly matched to the radar center frequency and bandwidth can provide highly dispersive and much poorer overall coherence performance compared with other radome-antenna considerations, no matter how stellar the design is at the intended band. We note a maximum drop in the mean coherence over all established example operating parameters of about 0.02 for a UHF radome design at Ku-band, with most mean coherence values for the various examined radome-antenna configurations being about 0.96. Squinted collects will suffer greater decorrelation than broadside-only collects. The amount of yaw of the radome with platform body angle changes influences decorrelation as well. While radome decorrelation values may seem small, the radome is a part of a larger system coherence budget, which requires that the amount of tolerable radome decorrelation be considered within the radar and mission trade space, whether the radome can be co-designed or modified for the CCD radar system or not.

ACKNOWLEDGEMENTS

Sandia National Laboratories is a multi-program laboratory managed and operated by Sandia Corporation, a wholly owned subsidiary of Lockheed Martin Corporation, for the U.S. Department of Energy's National Nuclear Security Administration under contract DE-AC04-94AL85000.

REFERENCES

[1] Kozakoff, D. J., [Analysis of Radome-Enclosed Antennas, 2nd Ed.], Artech House, Boston, MA, (2010).
[2] Tice, T. E., et al., "Techniques for Airborne Radome Design," Air Force Avionics Laboratory Report, AFAL-TR-66-391, 1, (1966).
[3] Walton, Jr., J. D., et al., "Techniques for Airborne Radome Design," Air Force Avionics Laboratory Report, AFAL-TR-66-391, 2, (1966).
[4] MatWeb, LLC., "Materials Database," (1996-2014), www.matweb.com.
[5] Military Specification, "Core Material, Plastic Honeycomb, Laminated Glass Fabric Base, for Aircraft Structural and Electronic Applications," Navy - AS, MIL-C-8073D, (1973).
[6] A. W. Doerry, "SAR Data Collection and Processing Requirements for High Quality Coherent Change Detection," Proc. of SPIE, 6947, 694706-1, (2008).
[7] H. A. Zebker and J. Villasenor, "Decorrelation in Interferometric Radar Echoes," IEEE Transactions on Geoscience and Remote Sensing, 30, 5, (1992).
[8] Bickel, D. L., "SAR Image Effects on Coherence and Coherence Estimation," Sandia National Laboratories Report, SAND2014-0369, (2014).
[9] A. W. Doerry, "Performance Limits for Synthetic Aperture Radar, 2nd Ed.," Sandia National Laboratories Report, SAND2006-0821, (2006).
[10] W. G. Carrara, R. S. Goodman, and R. M. Majewski, [Spotlight Synthetic Aperture Radar Signal Processing Algorithms], Artech House, Boston, MA, (1995).
[11] F. T. Ulaby, R. K. Moore, and A. K. Fung, [Microwave Remote Sensing III], Artech House, Boston, MA, (1986).
[12] U.S. Department of Commerce National Climatic Data Center and National Oceanographic and Atmospheric Administration, "Integrated Global Radiosonde Archive," (2015), http://www.ncdc.noaa.gov/oa/climate/igra/.
[13] Military Specification, "General Specification for Radomes," Air Force - 11, MIL-R-7705B, (1975).
[14] A. W. Doerry, "Bandwidth Requirements for Fine Resolution Squinted SAR," Proc. of SPIE, 4033, 2, (2000).